***Review paper***

# Chemical and Electrochemical Deposition of Ag onto Si for Fabrication of Si Nanowires and the Seebeck Effect Characterization


## ABSTRACT

In this work, vertically aligned porous Si nanowire (SiNW) arrays were successfully fabricated on two sides of an n-type Si wafer substrate. Ag nanoparticles (NPs) were first deposited onto the Si substrate via two different deposition methods, chemically and electrically (cyclic voltammetry), afterwards the metal assisted chemical etching (MaCE) technique was implemented to fabricate the SiNWs. The thermoelectric property of the SiNWs/Si/SiNWs structure was characterized by the Seebeck coefficient (S) which was measured at room temperature. Our results show a higher S when Ag NPs were electrodeposited onto the Si wafer piece compared to chemical deposition. The S enhancement is $\sim$3 times and $\sim$2 times in comparison to that of bulk Si and Ag chemical deposition samples, respectively. The electrodeposition created a strong adhesion between the Ag NPs and Si substrate which ensured a more uniform dispersed SiNWs producing a higher S. The improved thermoelectric performance coupled with electrodeposition of Ag indicates that the SiNWs/Si/SiNWs structure is an excellent candidate for the application in high-performance thermoelectric devices.


Key words: Silicon, metal assisted chemical etching, silver deposition, thermoelectrics.

## INTRODUCTION

Thermoelectric (TE) materials offer the opportunity for direct conversion of heat into electrical power for any temperature differences. This phenomenon plays a crucial role in solving today's energy problems such as energy shortage and pollution [1–4]. Furthermore, in medical applications, TE materials use body heat to generate power for devices such as biosensors and

wearables [5–7]. The effectiveness of a TE material is best described in terms of a dimensionless TE figure of merit, $ZT = \frac{S^2\sigma T}{k}$ where $S = \frac{\Delta V}{\Delta T}$, $\sigma$, $T$, and $k$ are the Seebeck coefficient, the electrical conductivity, the absolute temperature, and the thermal conductivity, respectively [8]. A material with a very low $k$, a large S exposed to a small $\Delta T$, and a large $\sigma$ yields a maximum figure of merit. However, for a material to meet all these conditions simultaneously remains today's ongoing research challenge.

Semiconducting materials are often used as TE materials because of their high power factors ($S^2\sigma$) [9]. From all of the following researched semiconducting materials Si [9–13], Ge [15], Bi [7, 15, 16], SiGe [18], BiTe [18–20], and PbTe [22], Si remains the highest of research interest because of its nontoxicity, biocompatibility, good stability under high temperatures, abundant Si resource, and its interface compatibility with Si-based electronic devices [11, 21]. Despite Si's high thermal conductivity ($k = 148\frac{W}{mK}$), it has been reported that rough silicon nanowires (SiNWs) have a high reduction in $k$ compared to bulk Si [9, 10, 22]. It has too been reported that porosity on a nanomaterial can reduce the thermal conductivity [13]. A single SiNW [10] as well as an array of ≈ 100 SiNWs [14] have both reported a $ZT \approx 1$, making it a practical TE material [3]. There are two different approaches in fabricating SiNWs, the growth and etching approach. SiNWs that are typically obtained by the growth approach consists of assembling the nanowire, atoms at a time, through a mechanism called vapor-liquid-solid (VLS) using Au as a catalyze [23–25]. On the other hand, the etching approach consist of removing matter, atoms at a time, forming a nanowire. The etching approach has an advantage over growth because of its nanowire size (diameter and length) and its nanostructure organization at the surface of the silicon [27]. An example of an etching approach is the metal assisted chemical etching (MaCE) technique which is a popular fabrication technique because of its simplicity,

low-cost, and its ability to control nonstructural parameters such as SiNWs' orientation, diameter, length, cross-sectional shape [27, 28].

In this work, arrays of SiNWs were successfully synthesized by first depositing Ag nanoparticles (NPs) onto pieces of a n-type Si wafer via two different depositions, chemically and electrically. Secondly, implementing the MaCE technique to fabricate the SiNWs and creating an overall SiNWs/Si/SiNWs structure. The thermoelectric property of the fabricated SiNWs/Si/SiNWs structure was characterized by the Seebeck coefficient (S). This work investigated the S comparison of Ag chemical deposition verses electrodeposition and our results show a higher S outcome when Ag NPs are electrodeposited onto the Si substrate.

## MATERIALS AND EXPERIMENTAL PROCEDURES

*Preparation of SiNWs*

The deposition of Ag NPs onto As-doped <100> n-type Si wafer pieces was performed by two methods, chemical deposition and electrodeposition. Before the deposition of Ag, the five Si pieces used were cleaned in acetone and ethanol, followed by a 1 min pre-soak in a 4.8 M HF solution to remove any possible $SiO_2$ layers coated on the outside of the Si pieces. They were later rinsed with $H_2O_2$ followed by de-ionized water. Each piece was finally placed on a paper towel and left to air dry under room temperature. Chemical deposition of Ag onto the Si surface was performed on four of the five clean Si wafer pieces were chemically deposition with Ag by immersing the pieces in a solution of 0.01 M $AgNO_3$ and 4.8 M HF for 1 min. Afterward, three of the four Si pieces with Ag NPs were MaCE in a 0.2 M $H_2O_2$ and 4.8 M HF solution, fabricating the SiNWs. After the three pieces were etched for 15, 30, and 60 mins, respectively they were removed and post-treated with de-ionized water to wash away any remaining residue.

On the last remaining clean Si piece, Ag NPs were electrodeposited via a cyclic voltammetry deposition for two cycles in a three-electrolytic cell. An Ag/AgCl (saturated KCl) electrode was used as both the reference and counter electrodes, and the Si piece as the working electrode. All potential in this study was measured with respect to the Ag/AgCl and both electrodes were submerged in a 0.6 M $HNO_3$ aqueous electrolyte solution. The working electrode was subjected to potential cycling from -5.0 to 1.0 V with an initial potential of 0 V at a rate of 10 mV $s^{-1}$ until the second reduction sweep was achieved. This Si piece was next etched for 60 mins in a 0.2 M $H_2O_2$ and 4.8 M HF solution and post-treated with de-ionized water. After the completion of the MaCE process, each sample takes on a SiNWs/Si/SiNWs structure. All of the above procedures were performed under room temperature.

*Characterization*

The cyclic voltammetry deposition was carried out by connecting the three-electrolytic cell to a CHI 440C electrochemical workstation which measured and controlled the electrochemical parameters. The morphology of the SiNWs was observed using scanning electron microscope (SEM, Jeol JSM-6010PLUS/LA) with an accelerating voltage of 20.0 kV. The composition of the nanostructure was determined by energy dispersive X-ray spectroscopy (EDS). The S of the SiNWs/Si/SiNWs was measured at room temperature using an in-house built experimental apparatus consisting of a Talboys Basic Mini Aluminum Top Hot Plate, UEi INF 165 digital infrared thermometer, and the CHI 440C electrochemical workstation set to measure an open circuit voltage.

**RESULTS AND DISCUSSION**

*Chemical Deposition*

Figure 1 illustrates the MaCE technique. In both chemical and electric depositions, the attached $Ag^+$ ions acquire electrons from the Si valence band and are reduced to form Ag NPs (nucleation). These NPs are soon injected into the Si creating oxidation (SiO or $SiO_2$) which is dissolved by HF. This continuous formation and dissolvent of SiO or $SiO_2$ underneath the Ag NPs allow the Ag NPs to sink inwards into the Si wafers (etching) forming tunnels and creating porous structures [28]. Due to the high density of Ag NPs, multiple tunnels could combine to form one wider tunnel [12]. The depth of these tunnels thus the length of the SiNWs increase approximately linearly with etching time [27, 29]. As the Ag NP injects into the Si, it losses some of its ions ($Ag^+$) and diffusing into directions with low $Ag^+$ concentration. These $Ag^+$ ions can meanwhile be reduced to Ag NPs and/or Ag dendrites on the surface of the SiNWs. This loss of $Ag^+$ ions explanation is left out in Figure 1.

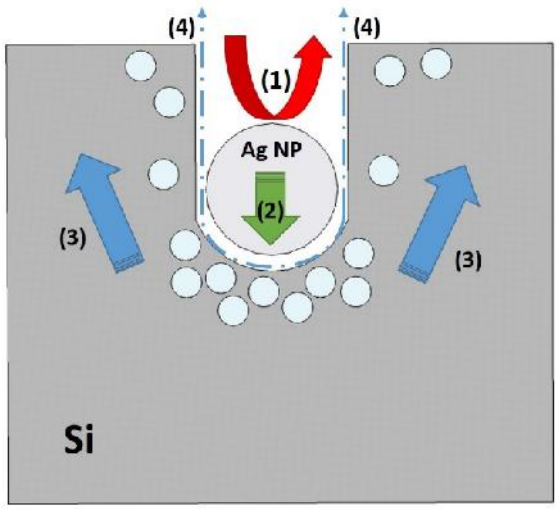


**Figure 1** The MaCE process: (1) the redox reaction of $H_2O_2$ and Ag; (2) the injection of the holes into the Si generated during the reduction, the highest hole concentration is located underneath the Ag NP; (3) the diffusion of holes to Si sidewalls and surfaces; and (4) the removal of oxidized Si by HF.

*Cyclic voltammetry deposition*

Previous studies have shown that continuous cyclic voltammetry could produce more uniform and well-dispersed metal NPs with higher distribution density compared to metal NPs that were electrodeposited via constant potential [31]. Thus a cyclic voltammetry was used to deposit Ag NPs onto Si. The cyclic voltammogram (CV) of SiAg is presented in Figure 2. The insert potential figure shows that a cycle starts with oxidation of Ag (-5 – 0 V) and ends with the redox of $Ag^+$ (0 – 1V). The arrows on the CV indicate the direction of the scan, and the blue and red lines are the 1st and 2nd cycle, respectively. There is a series of anodic events labeled A1 and A2 that were attributed to the oxidation of Ag. The explanation of the two consecutive oxidative peaks, A1 and A2, are attributed to hydroxides and $Ag_2O$, and remains a topic of ongoing research [30–32]. Peak A3 corresponds to the oxygen evolution. On the cathodic event, the current increases rapidly towards the C1 peak, indicating the redox couple of peaks A1 and A2, and the deposition of $Ag^+$ ions onto the Si piece. As described above, these $Ag^+$ nuclearize into Ag NPs on the surface of the Si substrate. The CV changes in currents between the two cycles are credited to the increase in surface roughness and in the number of the available nucleation and growth sites [33].

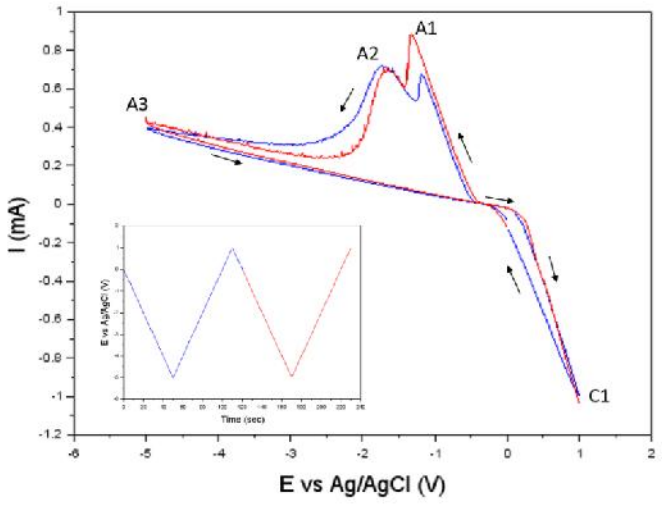


**Figure 2** Cyclic voltammogram of SiAg at a scan rate of 10 mV $s^{-1}$ in a 0.6 M $HNO_3$ aqueous electrolyte solution. Insert shows the potential applied to the electrodes (blue and red indicate 1st and 2nd cycle, respectively).

*Morphology characterization*

The SEM images in Figure 3 are the morphologies of the SiAg samples etched for 0 (a, SiAg), 15 (b, SiAg-15), 30 min (c, SiAg-30), and 60 min (d, SiAg-60). The SiAg-60 shown here is the SEM image of the sample with electrodeposited Ag NPs. All SEM images were taken looking down onto the <100> plane of each sample. In Figure 3a, the uniform distribution of Ag NPs is shown by the white dots. The darker shades of black shown in Figure 3 b-d indicate porosity on the Si. This shows the formation of tunnels downward towards the Si substrate. The wider and longer shades of black illustrates the combination of multiple tunnels as described previously. Furthermore, the bright white dots are the tips of the SiNWs. To verify the chemical composition of the SiNWs/Si/SiNWs nanostructure, the insert images on Figure 3 show the results of the qualitative analysis of the elements using the EDS technique. This EDS figure confirms that Ag elements were attached to the Si surface before etching on all samples. All samples show similar counts of Ag to Si except for SiAg-30 which is due to the improper removal of Ag dendrites from the surface during post treatment and/or excess $Ag^{+}$ ions were present in the solution that were released by the SiAg-15 sample, since both were etched in the same solution in the same time.

The SEM image in Figure 4 is the morphology of the sample that was etched for 60 mins after chemically depositing Ag NPs (SiAg*). The insert EDS image in Figure 4 shows no Ag elements and confirms the oxidative nanostructure on the surface of the Si. This indicates the possibility that the Ag NPs did not fully bond onto the Si substrate causing the Ag NPs to deposit into the $H_2O_2$ and HF solution during the etching process. The 60 min etching time could too cause the SiNWs to break off from the Si substrate dissolving into the etching solution.

**Figure 3** Morphological SEM images from top-view, looking down onto the SiNWs, of (a) SiAg, (b) SiAg-15, (c) SiAg-30, and (d) SiAg-60. The insets are the EDS analysis results.

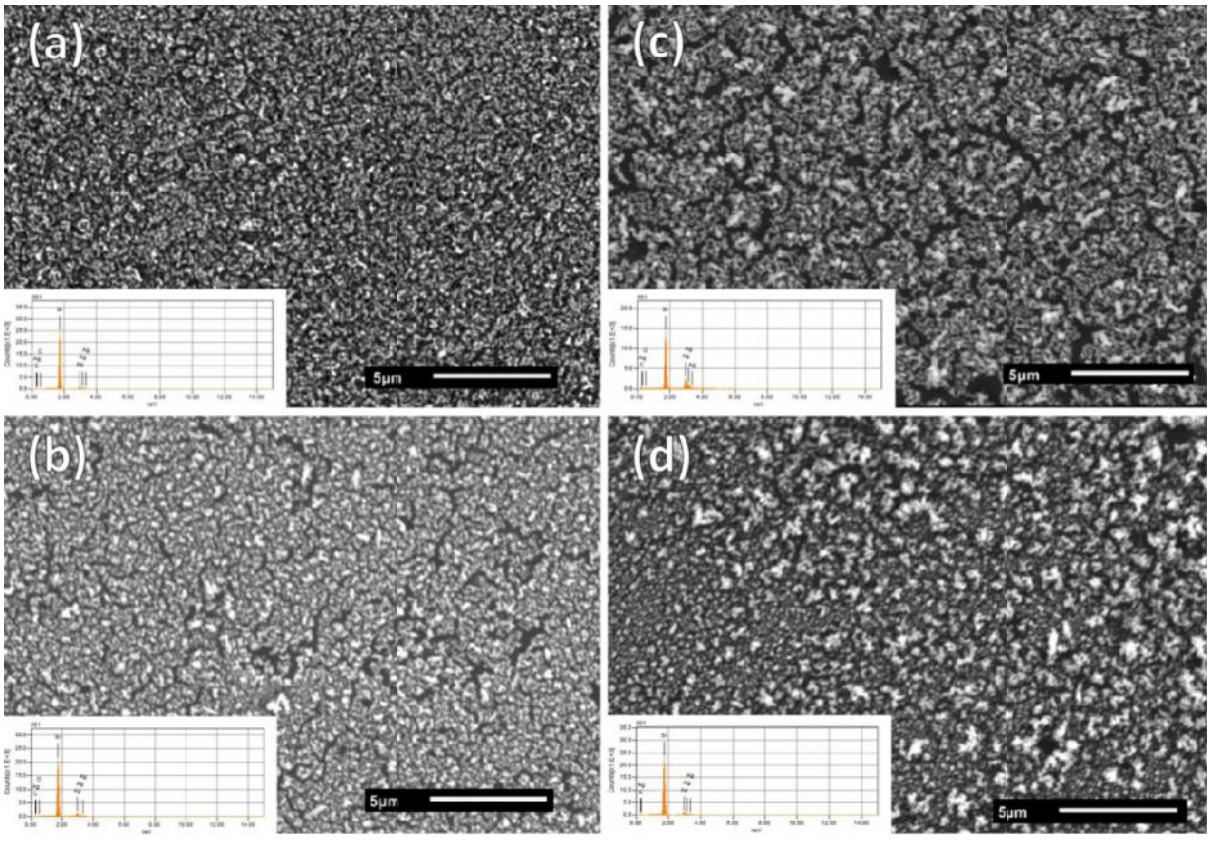

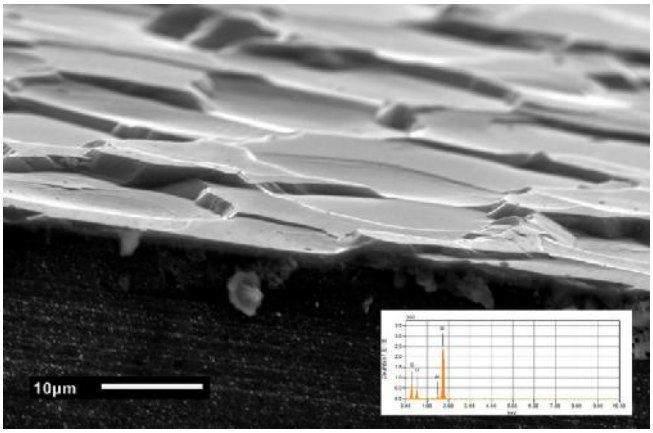


**Figure 4** SEM image of SiAg* which shows the oxidation on the top of the Si substrate. The insert image is the EDS analysis of this sample and confirms that no Ag is present.

*Seebeck coefficient characterization*

Figure 5 shows a schematic diagram of our experimental apparatus. One end of the sample was sandwiched in between two aluminum cylinders and the other end was free-standing, similar to a cantilever. The bottom aluminum cylinder was heated using a hot plate and an insulator block was added underneath the free-standing section of the sample to prevent any heat convection from the hot plate. Using a digital infrared thermometer, temperature measurements were taken at the start ($T_H$) and end ($T_C$) of the cantilever (indicated by the red dots on Figure 5), allowing measurement of temperature differences $\Delta T = T_H - T_C$. This digital infrared thermometer measured the thermal radiation frequency distribution that each sample gave off, using this measurement it lastly calculates the temperature of the sample at an indicated point. Thus the temperature measured is a combination of both the bulk Si and top SiNWs array. When $T_H$ remained constant, an open circuit voltage ($\Delta V$) was measured as a function of time for 90 seconds. The Al foil served purposely as an electrode for measuring voltage.

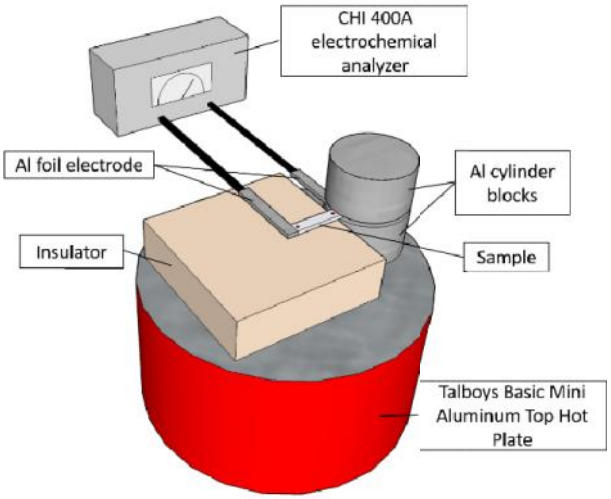


**Figure 5** A schematic diagram of our in-house built Seebeck coefficient measurement apparatus. The red dots on the sample indicates where the temperature measurement were taken.

Figure 6a shows $S_{SiAg}$ with respect to time which has an average measurement of $0.09\frac{mV}{K}$ with a standard deviation of $0.04\frac{mV}{K}$. This result shows a 8-fold reduction in the S when a layer of Ag NPs, $S_{Ag} \approx 1.3\frac{\mu V}{K}$ [35], deposited onto the surface of bulk n-type Si, $S_{bulk} \approx 0.74\frac{mV}{K}$ [36], $S_{bulk} \approx 8\,S_{SiAg}$. $S_{SiAg-15}$ and $S_{SiAg-30}$ have an average measurement of $0.98\frac{mV}{K}$ (standard deviation of $0.02\frac{mV}{K}$) and $0.91\frac{mV}{K}$ (standard deviation of $0.05\frac{mV}{K}$), respectively as shown in Figure 6b and 6c. It is documented that increasing etching time improves the thermoelectric properties [12], contradicting our $S_{SiAg-30}$ result. The significantly lower $S_{Ag}$ compared to $S_{Si}$ and the Ag to Si counts on SiAg-30 sample as discussed in the EDS studies above resulted in a 7% decrease from $S_{SiAg-15}$ to $S_{SiAg-30}$. Despite existing SiNWs, Ag dendrites and $Ag^{+}$ ions remained on the sidewalls and tips of the SiNWs causing the slight degeneration in S. Another possibility for the slight degradation has to deal with the Talboy's hot plate. The hot plate did not have the ability to keep its temperature stable, it functions by undergoing through heating and cooling cycles. Figure 6c shows an example of the hot plate entering a cooling cycle indicated by

the downward trend of $S_{SiAg-30}$. In addition, the $S_{SiAg^*}$ was measured (average of $0.71\frac{mV}{K}$ and standard deviation of $0.02\frac{mV}{K}$) and resulted $0.03\frac{mV}{K}$ below $S_{bulk}$ which validates the non-existent NWs.

Figure 6d shows the measured $S_{SiAg-60}$ which resulted in a mean of $1.90\frac{mV}{K}$ and a standard deviation of $0.09\frac{mV}{K}$. There is a 3-fold improvement from $S_{bulk}$, $S_{SiAg-60} \approx 3\, S_{bulk}$ and a 2-fold improvement from SiAg-15 and SiAg-20, $S_{SiAg-60} \approx 2\, S_{SiAg-15} \approx 2\, Si_{SiAg-30}$. Table 1 shows the above S results. The improvement of electrodeposition from chemical deposition is

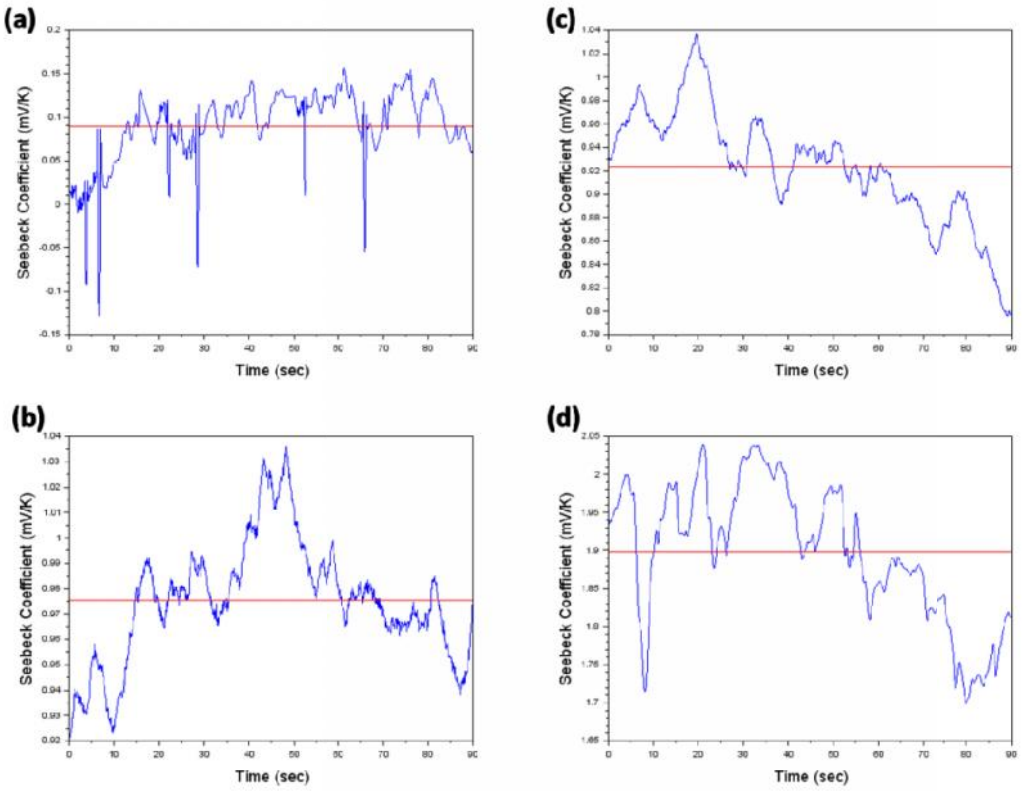


**Figure 6** Seebeck coefficient measuring results of (a) SiAg, (b) SiAg-15, (c) SiAg-30, and (d) SiAg-60. The red horizontal line on the plots indicate the location of the mean Seebeck coefficient for their respective sample.

associated with the adhesion of the NPs onto the Si substrate. In a previous study, it was found that Au, a noble metal like Ag, which was electrodeposited onto a Si substrate exhibits a much

larger specific energy compare to a sputter deposition method [37]. Moreover, this same study found that the different behavior suggests that the mechanical interlocking between the Si and NPs contribute to a significant extent to the adhesion [37]. This same argument applies to this study. There existed a strong bond between the Ag NPs and the Si substrate which ensured that the proper etching process was performed. As a result, SiAg-60 produced an array of nanowires that was more well uniformly dispersed compare to SiAg-15 and SiAg-30, resulting in a higher S.

**Table 1** Summary of measured thermoelectric property results

| Sample | Ag Deposit Time | Etch. Time | ΔT (K) | ΔV (mV) | S (mV/K) |
|---|---|---|---|---|---|
| **SiAg** | 1 min | 0 min | 2.0 | 0.18 | 0.09 |
| **SiAg-15** | 1 min | 15 min | 2.0 | 1.95 | 0.98 |
| **SiAg-30** | 1 min | 30 min | 1.2 | 1.09 | 0.91 |
| **SiAg-60** | Electro. (2 cycles) | 60 min | 1.8 | 3.37 | 1.90 |

## CONCLUSION

SiNWs were successfully synthesized by first depositing Ag NPs by two methods, via chemical deposition and cyclic voltammetry deposition, onto a piece of n-type Si wafer and secondly implementing the MaCE technique. The S of the bulk SiNWs/Si/SiNWs were investigated and our results show a significant increase in S when Ag NPs are electrodeposited due to the strong bond between the Ag NPs and the Si substrate, $S_{SiAg-60} \approx 3\,S_{bulk}$. Moreover, research needs to be done to determine the $S_{SiNWs}$ of samples similar to SiAg-60. Since $\Delta T = \Delta T_{SiNWs} + \Delta T_{Si}$, the values of $\Delta T_{SiNWs}$ and $\Delta T_{bulk}$ are determined only if the ratio of

$\Delta T_{SiNWs}$: $\Delta T_{bulk}$ was known. However, it is difficult to obtain these temperature differences experimentally or numerically because of the combination of heat conduction and convection, thus a finite element model will be ideal to approximate these values. Nevertheless, based on the results presented in this study, the thermoelectric performance improvement of the bulk SiNWs/Si/SiNWs, which are fabricated by using a combination of electrodeposition of Ag NPs and MaCE, is promising for the next generational thermoelectric devices.

**REFERENCES**

[1] F. DiSalvo, "Thermoelectric cooling and power generation," *Science*, vol. 285, no. 5428, pp. 703–6, 1999.

[2] L. E. Bell, "Cooling, Heating, Generating Power, and Recovering Waste Heat with Thermoelectric Systems," *Science*, vol. 321, no. September, pp. 1457–1461, 2008.

[3] G. J. Snyder and E. S. Toberer, "Complex thermoelectric materials," *Nat. Mater.*, vol. 7, no. 2, pp. 105–114, 2008.

[4] Y. C. Wang, C. S. Dai, and S. X. Wang, "Theoretical analysis of a thermoelectric generator using exhaust gas of vehicles as heat source," *Appl. Energy*, vol. 112, pp. 1171–1180, 2013.

[5] J. Olivo, S. Carrara, G. De Micheli, and G. De Micheli, "Energy Harvesting and Remote Powering for Implantable Biosensors," *IEEE Sens. J.*, vol. 11, no. 7, pp. 1573–1586, 2011.

[6] J.-H. Bahk, H. Fang, K. Yazawa, and A. Shakouri, "Flexible thermoelectric materials and device optimization for wearable energy harvesting," *J. Mater. Chem. C*, vol. 3, pp. 10362–10374, 2015.

[7] V. Leonov, B. Gyselinckx, and C. Hoof, "Wearable self-powered wireless devices with thermoelectric energy scavengers," *Integr. Issues Miniaturized Syst. - MOMS, MOEMS, ICS Electron. Components (SSI), 2008 2nd Eur. Conf. Exhib.*, pp. 1 – 8, 2008.

[8] M. S. Dresselhaus, Y. M. Lin, O. Rabin, and G. Dresselhaus, "Bismuth nanowires for thermoelectric applications," *Microscale Thermophys. Eng.*, vol. 7, no. 3, pp. 207–219, 2003.

[9] A. P. Gonçalves, E. B. Lopes, G. Delaizir, and C. Godart, "Semiconducting glasses: A new class of thermoelectric materials?," *AIP Conf. Proc.*, vol. 1449, pp. 347–350, 2012.

[10] A. I. Hochbaum, R. Chen, R. D. Delgado, W. Liang, E. C. Garnett, M. Najarian, A. Majumdar, and P. Yang, "Enhanced thermoelectric performance of rough silicon nanowires," *Nature*, vol. 451, no. 7175, pp. 163–167, 2008.

[11] D. Li, Y. Wu, P. Kim, L. Shi, P. Yang, and A. Majumdar, "Thermal conductivity of individual silicon nanowires," *Appl. Phys. Lett.*, vol. 83, no. 14, pp. 2934–2936, 2003.

[12] T. Zhang, S. Wu, J. Xu, R. Zheng, and G. Cheng, "High thermoelectric figure-of-merits from large-area porous silicon nanowire arrays," *Nano Energy*, vol. 13, pp. 433–441, 2015.

[13] J. M. Weisse, A. M. Marconnet, D. R. Kim, P. M. Rao, M. a Panzer, K. E. Goodson, and X. Zheng, "Thermal conductivity in porous silicon nanowire arrays.," *Nanoscale Res. Lett.*, vol. 7, no. 1, p. 554, 2012.

[14] A. I. Boukai, Y. Bunimovich, J. Tahir-Kheli, J.-K. Yu, W. A. Goddard, and J. R. Heath, "Silicon nanowires as efficient thermoelectric materials.," *Nature*, vol. 451, no. 7175, pp. 168–71, 2008.

[15] W. Huang, C. S. Koong, and G. Liang, "Theoretical Study on Thermoelectric Properties of Ge Nanowires Based on Electronic Band Structures," *Semicond. Semimetals*, vol. 31, no. 9, pp. 1026–1028, 2010.

[16] A. Boukai, K. Xu, and J. R. Heath, "Size-dependent transport and thermoelectric properties of individual polycrystalline bismuth nanowires," *Adv. Mater.*, vol. 18, no. 7, pp. 864–869, 2006.

[17] J. Heremans and C. Thrush, "Thermoelectric power of bismuth nanowires," *Phys. Rev. B*, vol. 59, no. 19, pp. 12579–12583, 1999.

[18] E. K. Lee, L. Yin, Y. Lee, J. W. Lee, S. J. Lee, J. Lee, S. N. Cha, D. Whang, G. S. Hwang, K. Hippalgaonkar, A. Majumdar, C. Yu, B. L. Choi, J. M. Kim, and K. Kim, "Large thermoelectric figure-of-merits from SiGe nanowires by simultaneously measuring electrical and thermal transport properties," *Nano Lett.*, vol. 12, no. 6, pp. 2918–2923, 2012.

[19] J. Lee, J. Kim, W. Moon, A. Berger, and J. Lee, "Enhanced seebeck coefficients of thermoelectric Bi 2Te 3 nanowires as a result of an optimized annealing process," *J. Phys. Chem. C*, vol. 116, no. 36, pp. 19512–19516, 2012.

[20] Y. X. Gan, M. J. Koludrovich, and L. Zhang, "Thermoelectric effect of silicon nano fi bers capped with Bi – Te nanoparticles," *Mater. Lett.*, vol. 111, pp. 126–129, 2013.

[21] H. Suh, H. Jung, C. M. Hangarter, H. Park, Y. Lee, Y. Choa, N. V. Myung, and K. Hong, "Diameter and composition modulated bismuth telluride nanowires by galvanic displacement reaction of segmented NiFe nanowires," *Electrochim. Acta*, vol. 75, pp. 201–207, 2012.

[22] G. Pennelli, "Review of nanostructured devices for thermoelectric applications," *Beilstein J. Nanotechnol.*, vol. 5, no. 1, pp. 1268–1284, 2014.

[23] L. Shi, "Thermal and Thermoelectric Transport in Nanostructures and Low-Dimensional Systems," *Nanoscale Microscale Thermophys. Eng.*, vol. 16, no. 2, pp. 79–116, 2012.

[24] R. S. Wagner and W. C. Ellis, "Vapor-Liquid-Solid Mechanism of Single Crystal Growth," *Appl. Phys. Lett.*, vol. 4, no. 89, 1964.

[25] L. Latu-Romain, C. Mouchet, C. Cayron, E. Rouviere, and J. P. Simonato, "Growth parameters and shape specific synthesis of silicon nanowires by the VLS method," *J.*

*Nanoparticle Res.*, vol. 10, no. 8, pp. 1287–1291, 2008.

[26] J. M. Redwing, X. Miao, and X. Li, "Vapor-Liquid-Solid Growth of Semiconductor Nanowires," in *Handbook of Crystal Growth: Thin Films and Epitaxy: Second Edition*, vol. 3, 2014, pp. 399–439.

[27] L. Latu-Romain and M. Ollivier, "Silicon Carbide One-dimensional Nanostructures (1)," in *Wiley-ISTE*, 2015, pp. 44–48.

[28] Z. Huang, N. Geyer, P. Werner, J. De Boor, and U. Gösele, "Metal-assisted chemical etching of silicon: A review," *Adv. Mater.*, vol. 23, no. 2, pp. 285–308, 2011.

[29] X. Li and P. W. Bohn, "Metal-assisted chemical etching in HF/H2O2 produces porous silicon," *Appl. Phys. Lett.*, vol. 77, no. 16, pp. 2572–2574, 2000.

[30] S. L. Cheng, C. H. Chung, and H. C. Lee, "A Study of the Synthesis, Characterization, and Kinetics of Vertical Silicon Nanowire Arrays on (001)Si Substrates," *J. Electrochem. Soc.*, vol. 155, no. 001, p. D711, 2008.

[31] Y. Chen, R. Kirankumar, C. Kao, and P. Chen, "Electrochimica Acta Electrodeposited Ag , Au , and AuAg nanoparticles on graphene oxide-modi fi ed screen-printed carbon electrodes for the voltammetric determination of free sul fi de in alkaline solutions," vol. 205, pp. 124–131, 2016.

[32] L. C. Nagle, A. J. Ahern, and L. D. Burke, "Some unusual features of the electrochemistry of silver in aqueous base," *J. Solid State Electrochem.*, vol. 6, no. 5, pp. 320–330, 2002.

[33] T. U. Hur and W. S. Chung, "The Mechanism of Silver(I) Oxide to Silver(II) Oxide Formation on Polycrystalline Silver Electrodes in 8 M KOH Solution," *J. Electrochem. Soc.*, vol. 152, no. 5, pp. A996–A1000, 2005.

[34] A. J. Marenco, D. B. Pedersen, S. Wang, M. W. P. Petryk, and H.-B. Kraatz, "Electrochemical properties of gas-generated silver nanoparticles in the presence of cyano- and chloride-containing compounds.," *Analyst*, vol. 134, pp. 2021–2027, 2009.

[35] N. Cusack and P. Kendall, "The Absolute Scale of Thermoelectric Power at High Temperature," *Proc. Phys. Soc.*, vol. 72, no. 5, pp. 898–901, 1958.

[36] E. Krali and Z. A. K. Durrani, "Seebeck coefficient in silicon nanowire arrays," *Appl. Phys. Lett.*, vol. 102, no. 14, 2013.

[37] J. Zhu, P. Henry, M. L. Weaver, M. L. Reed, and G. Zangari, "Enhanced adhesion of au films by electrodeposition onto porous Si," *J. Electrochem. Soc.*, vol. 160, no. 11, pp. D507–D512, 2013.